

V. Chandrasekaran · A. Cain · T. Nishida
L. N. Cattafesta · M. Sheplak

Dynamic calibration technique for thermal shear-stress sensors with mean flow

Received: 7 November 2003 / Accepted: 23 December 2004 / Published online: 11 May 2005
© Springer-Verlag 2005

Abstract This paper presents the development of a dynamic calibration technique for thermal shear-stress sensors using acoustic plane wave excitation. The technique permits the independent variation in the mean and fluctuating shear stresses. The theoretical development and the practical implementation of the technique are presented. The studied configuration has the capability to dynamically calibrate shear-stress sensors up to 20 kHz. An illustrative application of this technique to an uncompensated silicon micromachined thermal shear-stress sensor operated in constant current mode is discussed. Specifically, the sensor has been statically calibrated over a range of wall shear stress from 7 to 80 mPa. A dynamic calibration of the sensor

over a range of 2–12 mPa has been performed up to 7 kHz.

1 Introduction

The measurement of wall shear stress in a turbulent flow provides insight into complex flow phenomena, including viscous drag, flow separation/reattachment and transition to turbulence. At high Reynolds numbers, the spatial length scale of the fluid structures of interest can be on the order of hundreds of microns or less, necessitating a sensor element size of the same order to minimize spatial averaging. Also, to accurately capture the complete spectrum of turbulent fluctuations, a shear-stress sensor with usable bandwidth of over 1 kHz is required. For example, it is well known that the ratio of the boundary layer thickness δ to the Kolmogorov microscale η scales as

$$\frac{\eta}{\delta} \sim Re_{\delta}^{-3/4}, \quad (1)$$

where $Re_{\delta} = u\delta/\nu$ is the Reynolds number, u is the typical eddy velocity scale ($u/U \sim 10^{-2}$), U is the boundary layer edge velocity, and ν is the kinematic viscosity (Tennekes and Lumley 1972). Similarly, the ratio of the convective time scale to the Kolmogorov time scale T scales as

$$\frac{Tu}{\delta} \sim Re_{\delta}^{-1/2}. \quad (2)$$

For a relatively low Reynolds number, low-speed turbulent boundary layer possessing an edge velocity of $U = 50$ m/s and a thickness $\delta = 5$ cm, the Kolmogorov scales are $\eta = 100$ μ m and $T = 2$ ms. The stringent spatial and temporal resolution requirements naturally point towards microfabricated sensors as a means of achieving the required level of performance.

Conventional as well as micromachined shear stress measurement techniques can be broadly classified into

V. Chandrasekaran · L. N. Cattafesta · M. Sheplak
Department of Mechanical and Aerospace Engineering,
University of Florida, 231 MAE-A Building,
PO Box 116250, Gainesville, FL 32611-6250, USA
E-mail: cattafes@ufl.edu
Tel.: +1-352-8463017
Fax: +1-352-3927303
E-mail: sheplak@ufl.edu
Tel.: +1-352-3923983
Fax: +1-352-3927303

Present address: V. Chandrasekaran (✉)
Gas Turbine Laboratory,
Massachusetts Institute of Technology,
60 Vassar Street, 31-261b, Cambridge, MA 02139, USA
E-mail: cvraman@alum.mit.edu
Tel.: +1-617-9351709
Fax: +1-508-2362430

A. Cain · T. Nishida
Department of Electrical and Computer Engineering,
University of Florida, 223 Benton Hall,
PO Box 116200, Gainesville, FL 32611-6200, USA
E-mail: nishida@ufl.edu
Tel.: +1-352-3926774
Fax: +1-352-3928671

Present address: A. Cain
Air Force Research Laboratory, AFRL/MLPO,
Wright-Patterson Air Force Base, Dayton,
OH 45433-7707, USA

Report Documentation Page

Form Approved
OMB No. 0704-0188

Public reporting burden for the collection of information is estimated to average 1 hour per response, including the time for reviewing instructions, searching existing data sources, gathering and maintaining the data needed, and completing and reviewing the collection of information. Send comments regarding this burden estimate or any other aspect of this collection of information, including suggestions for reducing this burden, to Washington Headquarters Services, Directorate for Information Operations and Reports, 1215 Jefferson Davis Highway, Suite 1204, Arlington VA 22202-4302. Respondents should be aware that notwithstanding any other provision of law, no person shall be subject to a penalty for failing to comply with a collection of information if it does not display a currently valid OMB control number.

1. REPORT DATE 2005		2. REPORT TYPE		3. DATES COVERED 00-00-2005 to 00-00-2005	
4. TITLE AND SUBTITLE Dynamic calibration technique for thermal shear-stress sensors with mean flow				5a. CONTRACT NUMBER	
				5b. GRANT NUMBER	
				5c. PROGRAM ELEMENT NUMBER	
6. AUTHOR(S)				5d. PROJECT NUMBER	
				5e. TASK NUMBER	
				5f. WORK UNIT NUMBER	
7. PERFORMING ORGANIZATION NAME(S) AND ADDRESS(ES) University of Florida, Department of Electrical and Computer Engineering, Gainesville, FL, 32611				8. PERFORMING ORGANIZATION REPORT NUMBER	
9. SPONSORING/MONITORING AGENCY NAME(S) AND ADDRESS(ES)				10. SPONSOR/MONITOR'S ACRONYM(S)	
				11. SPONSOR/MONITOR'S REPORT NUMBER(S)	
12. DISTRIBUTION/AVAILABILITY STATEMENT Approved for public release; distribution unlimited					
13. SUPPLEMENTARY NOTES					
14. ABSTRACT					
15. SUBJECT TERMS					
16. SECURITY CLASSIFICATION OF:			17. LIMITATION OF ABSTRACT	18. NUMBER OF PAGES 10	19a. NAME OF RESPONSIBLE PERSON
a. REPORT unclassified	b. ABSTRACT unclassified	c. THIS PAGE unclassified			

direct and indirect methods. Several microfabricated shear-stress sensors of both the direct (Padmanabhan et al. 1996, 1997; Pan et al. 1999) and indirect (Oudheusden and Huijsing 1988; Liu et al. 1994, 1999; Cain et al. 2000) variety have been reported. The direct shear-stress sensors are tethered floating-element devices that employ piezoresistive (Ng 1990; Goldberg et al. 1994), optical (Padmanabhan et al. 1996, 1997) and capacitive (Schmidt et al. 1988; Pan et al. 1999) transduction mechanisms. Indirect shear-stress sensors are temperature-resistance transducers that operate on heat transfer analogies. Recently, Löfdahl and Gad-el-Hak (1999) presented a review of MEMS pressure and shear-stress sensors for turbulent flows. Naughton and Sheplak (2002) expanded that contribution by providing an updated list of references and discussing some of the current misconceptions and controversies involving the use of MEMS-based shear-stress sensors for quantitative measurements.

To accurately capture the complete spectrum of shear stress in a turbulent flow, a sensor should possess a known frequency response function. An ideal shear stress measurement system would possess equal static and dynamic sensitivities with a flat, minimum-phase frequency response over all frequencies. In practice, however, the inherent compliance, inertance and dissipation of the system limit the useful bandwidth of the sensor. For example, the usable bandwidth of a thermal shear-stress sensor is determined by the thermal inertia of the substrate (Bellhouse and Schultz 1967, 1968). Bellhouse and Schultz describe how the dynamic response is further complicated by the frequency dependent heat conduction into the substrate. This creates a low-frequency roll-off in the gain factor of the frequency response function, as well as a frequency dependent phase lag, resulting in unequal static and dynamic sensitivities. The low-frequency substrate conduction losses also limit electronic signal injection, commonly used in hot-wire anemometry, to providing qualitative information. Since the exact character of the system is unknown, the response of such a system to electronic signal injection is unclear. Consequently, electronic signal injection fails to yield an accurate estimate of the frequency response function (Freymuth 1981). Therefore, to minimize uncertainties in correlation and spectral analysis, an in situ dynamic calibration technique is required to determine the frequency response function.

A dynamic calibration technique for thermal shear-stress sensors requires a known mean and broadband shear stress input which, unfortunately, is difficult to realize in practice. Bellhouse and Schultz (1968) developed a dynamic calibration technique based on the streamwise oscillation of a small, flat plate containing a flush mounted sensor, thus effectively modulating the freestream velocity. This technique permitted a dynamic calibration range of 200–1200 Hz. Chew et al. (1998) have designed an experimental set up that uses Couette flow between a recessed rotating disc and a flat stationary disc to characterize the dynamic response of wall

mounted hot-wire and hot-film probes. This technique was used to dynamically calibrate flush mounted hot-film probes up to 2.5 kHz. One limitation to this calibration technique is that the mean shear stress and frequency of the disturbance are functions of the rotational speed for a fixed plate geometry and thus are not independently adjustable. More recently, a dynamic calibration technique utilizing acoustic waves to generate a known sinusoidal wall shear stress under zero-mean flow conditions has been reported (Sheplak et al. 2001). This technique was used for the dynamic calibration of a micromachined floating-element sensor that exhibits a linear response to shear stress. This procedure is not suitable for a thermal sensor that possesses a non-linear response and requires a mean flow to ensure forced convection of heat from the sensor. This paper presents the development of an acoustic calibration technique with independent variation in the mean and fluctuating shear stresses to enable static and dynamic calibration of thermal shear-stress sensors. The theoretical development and the practical implementation of the dynamic calibration technique are presented. The outline of the paper is as follows. The next section presents the theoretical background of the technique. This is followed by a proof-of-concept experiment using an uncompensated silicon micromachined thermal shear-stress sensor operated in the constant current mode. Finally, conclusions are drawn and suggestions for future work are given.

2 Background

The response of the hot film sensor to dynamic shear fluctuations is band-limited due to the inherent dissipative and storage mechanisms of the system. The energy balance of a hot film is similar to that of a conventional hot wire except for the frequency-dependent heat conduction into the substrate governed by the temperature gradient at the sensor/substrate interface. For the case of hot wires, the conduction of heat into the supporting prongs is negligible compared to the convective losses for length-to-diameter ratios of the order 1,000 (Perry et al. 1979). However, in the case of hot films, this conduction term is always significant and cannot be accurately modeled analytically due to the complex nature of the conjugated heat-transfer problem (Comte-Bellot 1976). This is even more complex for sensor designs possessing the thermal sensing element on a thin diaphragm that is stretched over a vacuum cavity (Liu et al. 1994, 1999; Cain et al. 2000).

It is known that thermal shear-stress sensors exhibit a non-linear response to shear stress. If the system can be modeled approximately as locally linear and time invariant, then a direct dynamic calibration is possible provided that a known fluctuating shear stress input can be produced. For the linearity assumption to hold, the shear stress perturbation (τ'_{wall}) must be sufficiently smaller than the established mean shear stress ($\bar{\tau}$), such

that $V'_\tau \cong (d\bar{V}/d\bar{\tau})\tau'_{\text{wall}}$, where V'_τ is the corresponding voltage fluctuation due to the fluctuating shear stress and $d\bar{V}/d\bar{\tau}$ is the local static sensitivity. In the following sections, the theoretical basis for the dynamic calibration using acoustic excitation in a square duct is presented.

2.1 Stokes layer excitation

The basic principle of this technique relies on the fact that the particle velocity of the acoustic waves must be zero at the wall due to the no-slip boundary condition. This leads to the generation of a frequency-dependent boundary layer thickness $\delta(\omega)$ and a corresponding wall shear stress $\tau'_{\text{wall}}(\omega)$. The non-dimensional thickness of this viscous region, known as the Stokes layer, is given by Pantou (1996) as

$$\frac{\delta(\omega)}{b} \approx 6.4 \sqrt{\frac{\nu}{\omega b^2}} \approx \frac{6.4}{\eta}, \quad (3)$$

where ω is the angular frequency, b is an appropriate length scale, and $\eta = \sqrt{\omega b^2/\nu}$ is the non-dimensional Stokes number.

Now consider a set of plane, traveling acoustic waves bounded by the walls of a rectangular duct of cross-section $2a \times 2b$ with ($a \geq b$), as shown in Fig. 1. The waves travel in the positive x -direction and induce a velocity perturbation in the fluid. For the case of purely traveling acoustic plane waves superimposed on a fully developed mean flow with centerline axial velocity $U \ll c$, where c is the isentropic speed of sound, the linearized compressible momentum equation in the axial direction reduces to the classic problem of a duct flow driven by an oscillatory pressure gradient (Sheplak et al. 2001). The unsteady momentum equation in differential form is given by

$$\frac{\partial u}{\partial t} = -\frac{1}{\rho} \frac{\partial p}{\partial x} + \nu \nabla^2 u, \quad (4)$$

where ρ is the density of the fluid, u the axial velocity, and p is the pressure. We assume that the acoustic wave is a traveling plane wave in the $+x$ direction

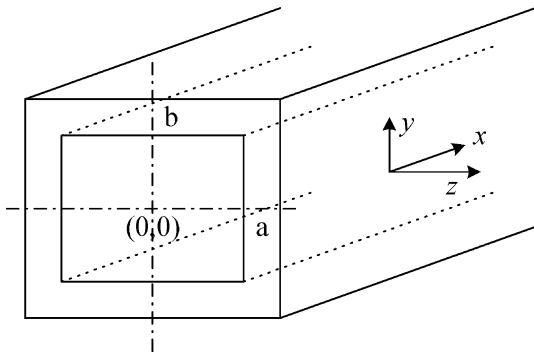


Fig. 1 Illustration of the acoustic waveguide and coordinate axes

$$p(x, t) = p' \text{Re} \left[e^{j(\omega t - kx - \pi/2)} \right], \quad (5)$$

where p' is the amplitude of the pressure perturbation, $\text{Re} []$ denotes the “real part of []”, $j = \sqrt{-1}$ and $k = \omega/c$ is the acoustic wavenumber. The assumed form in Eq. 5 translates to an oscillatory pressure gradient of the form

$$\frac{-1}{\rho} \frac{dp}{dx} = K \cos(\omega t - kx), \quad (6)$$

where $K = p'\omega/\rho c$. The velocity fluctuation is then of the form

$$u(x, y, z, t) = \text{Re} \left[u'(y, z) e^{j(\omega t - kx - \pi/2)} \right], \quad (7)$$

where $u'(y, z)$ is the complex amplitude of the velocity perturbation. The velocity fluctuation is subject to no-slip boundary conditions

$$u' = 0 \text{ at } z = \pm a \quad \text{and} \quad u' = 0 \text{ at } y = \pm b. \quad (8)$$

Solutions to this problem have been obtained by Drake (1965), Fan and Chao (1965), and O'Brien (1975). For example, the fluctuating velocity on the central plane of the duct ($z=0$) can be obtained from O'Brien's solution as the real part of

$$u'(y, 0, t) = \frac{p'}{\rho c} e^{j(\omega t - kx - (\pi/2))} \times \left\{ 1 - 2 \sum_{n=0}^{\infty} \frac{(-1)^n}{p_n} \left[\frac{\cos(p_n y/b)}{\cosh(\gamma_n a/b)} + \frac{\cosh(\mu_n y/b)}{\cosh(\mu_n)} \right] \right\}, \quad (9)$$

where $p_n = ((2n+1)/2)\pi$, $q_n = ((2n+1)/2)\pi(b/a)$, $\gamma_n = \sqrt{p_n^2 + j\eta^2}$, and $\mu_n = \sqrt{q_n^2 + j\eta^2}$. As $a/b \rightarrow \infty$, the solution tends to the well-known result of flow in a one-dimensional slot subject to an oscillatory pressure-gradient

$$u'(y, t) = \frac{p'}{\rho c} e^{j(\omega t - kx - \pi/2)} \left\{ 1 - \frac{\cosh((y/b)\eta\sqrt{j})}{\cosh(\eta\sqrt{j})} \right\}. \quad (10)$$

Figure 2 shows a plot of the normalized disturbance velocity magnitude along the centerline versus y/b for various Stokes numbers (η) in a square ($a=b$) duct. Both the one-dimensional and two-dimensional solutions are shown. Note that, for square ducts, there is a significant difference between the one-dimensional and two-dimensional solutions only for small Stokes numbers, which correspond to low-frequencies. As the Stokes number increases, the decreasing thickness of the Stokes layer becomes apparent, in accordance with Eq. 3.

It is important to note that Fan and Chao provide only the real part of the solution, which is insufficient to calculate the complex shear stress. In addition, by comparing the various solutions, the series solution in Drake was found to be inaccurate at high Stokes numbers, while the series solution provided by O'Brien does not converge at low Stokes numbers ($\eta < 10$).

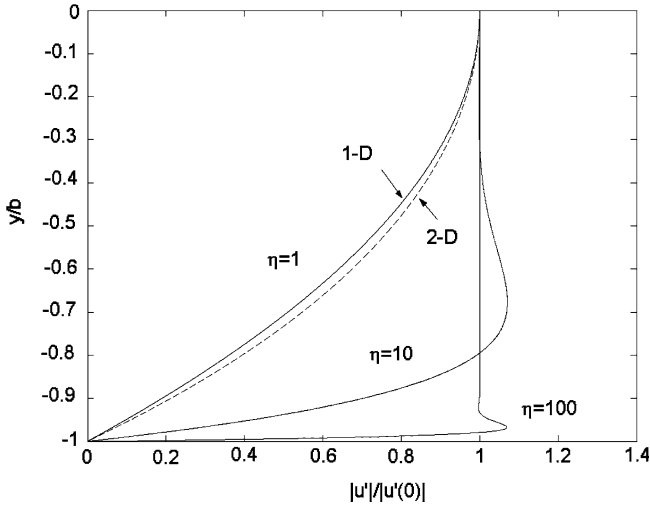


Fig. 2 Normalized magnitude of the velocity profile for various Stokes numbers (η) for one-dimensional and two-dimensional oscillatory rectangular duct flow

The fluctuating wall shear stress induced by the oscillatory pressure gradient at the center of the lower wall of the duct is given by

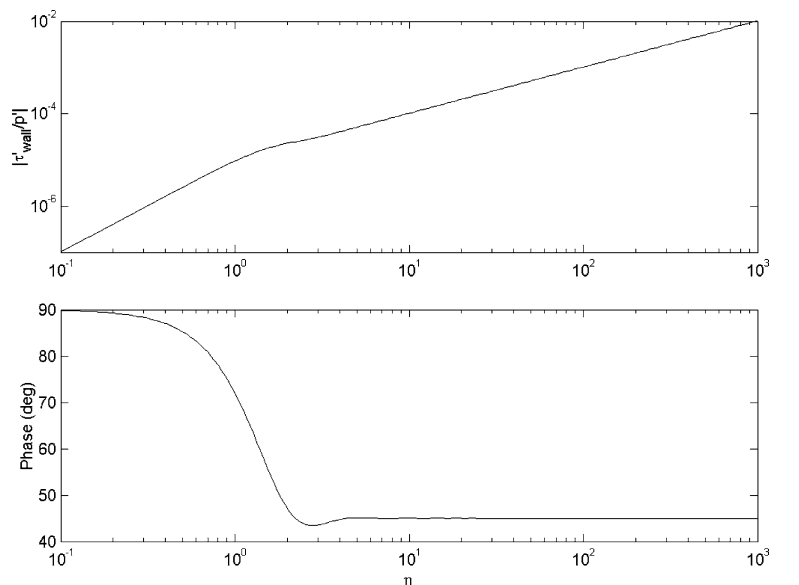
$$\tau'_{\text{wall2D}} = \rho v \frac{\partial u'}{\partial y} \Big|_{y=-b, z=0}. \quad (11)$$

Using the two-dimensional solution of O'Brien, Eq. 9, the complex fluctuating shear stress is

$$\tau'_{\text{wall2D}}(x, t) = \frac{-2vp'}{bc} e^{j(\omega t - kx - \pi/2)} \sum_{n=0}^{\infty} \frac{(-1)^n}{P_n} \times \left[\frac{p_n \sin(p_n)}{\cosh(\gamma_n a/b)} - \mu_n \tanh(\mu_n) \right]. \quad (12)$$

Since the one-dimensional and two-dimensional solutions are essentially identical for $\eta > 2$ (which as shown

Fig. 3 Magnitude and phase of the ratio of the fluctuating wall shear stress with respect to the pressure perturbation versus Stokes number (η) for one-dimensional oscillatory rectangular duct flow



later corresponds to the test conditions in the current study), the one-dimensional fluctuating wall shear stress is used

$$\tau'_{\text{wall1D}}(x, t) = \frac{p' \sqrt{j\omega v}}{c} e^{j(\omega t - kx - \frac{\pi}{2})} \tanh(\eta \sqrt{j}). \quad (13)$$

The above equation indicates that the amplitude of the shear stress is directly proportional to the product of the pressure perturbation and the square root of the excitation frequency. A simple algebraic manipulation shows that the fluctuating shear stress amplitude is proportional to the Stokes number since

$$\frac{p' \sqrt{\omega v}}{c} = \frac{\mu p'}{b \rho c} \eta. \quad (14)$$

Figure 3 shows the magnitude $|\tau'_{\text{wall}}/p'|$ and phase of the fluctuating shear stress with respect to the pressure perturbation for the one-dimensional case. The linear dependence versus Stokes number for $\eta > 1$ is revealed in the figure. Also note that for $\eta > 4$, the shear stress leads the pressure by 45° . Equation 13 is valid for plane progressive waves. At frequencies higher than the cut-on frequency of the acoustic waveguide, non-planar modes propagate within the duct, in addition to plane waves (Morse and Ingard 1968). Therefore, the bandwidth over which the solution is valid is limited by the waveguide characteristics of the tube. Furthermore, the acoustic waveguide must be properly terminated to eliminate reflected waves. Details of the experimental setup are provided below.

2.2 Plane wave propagation in a square duct

Wave propagation in a duct is governed by the solution to the wave equation. For one-dimensional wave propagation, the width of the duct must be small in

comparison to the acoustic wavelength. This can be verified by solving the wave equation in the duct (Dowling and Williams 1983)

$$\frac{1}{c^2} \frac{\partial^2 p'}{\partial t^2} - \nabla^2 p' = 0. \quad (15)$$

Consider the case of a square duct with rigid walls and cross-sectional length $2a$. The solution to the wave equation for an acoustic wave of frequency ω for the (m,n) mode is

$$p'(x, y, z, t) = \cos\left(\frac{m\pi(y+a)}{2a}\right) \cos\left(\frac{n\pi(z+a)}{2a}\right) \times [A_{mn} e^{j(\omega t - k_{mn}x)} + B_{mn} e^{j(\omega t + k_{mn}x)}], \quad (16)$$

where k_{mn} is the wave number given by the dispersion relation (Dowling and Williams 1983)

$$k_{mn} = \left(\frac{\omega^2}{c^2} - \frac{\pi^2}{4a^2}(m^2 + n^2)\right)^{1/2}. \quad (17)$$

When k_{mn} is real, Eq. 16 represents traveling waves propagating in the x -direction. If k_{mn} is imaginary, it represents non-propagating, evanescent waves whose magnitudes decay exponentially with axial distance. The fundamental mode (0,0) is a plane wave that will always propagate, but the higher order modes will become non-evanescent only when the cross-sectional width of the duct is greater than half of an acoustic wavelength, i.e., $2a > \lambda/2$. For example, the cut-on frequency for the first higher order modes of an 8.5 mm square tube is 20 kHz.

As mentioned earlier, the Stokes layer excitation is superimposed on an established mean flow. The static sensitivity of the sensor limits the magnitude of the shear stress perturbation that can be applied for the local linear assumption to hold. The determination of mean wall shear stress and the optimal sensor placement within a square duct are discussed in the remainder of this section.

2.3 Laminar flow in a square duct

For an incompressible, steady, laminar, fully developed flow in the square duct, the axial momentum conservation equation reduces to Poisson's equation

$$\frac{1}{\mu} \frac{dp}{dx} = \frac{\partial^2 u}{\partial y^2} + \frac{\partial^2 u}{\partial z^2}. \quad (18)$$

The solution to the above equation for the velocity distribution in the duct is (White 1991)

$$u(y, z) = -\frac{16a^2}{\mu\pi^3} \frac{dp}{dx} \sum_{n=1,3,\dots}^{\infty} (-1)^{\frac{n-1}{2}} \times \left[1 - \frac{\cosh(n\pi z/2a)}{\cosh(n\pi/2)}\right] \frac{\cos(n\pi y/2a)}{n^3}. \quad (19)$$

The corresponding wall shear stress ($y=a$) is

$$\tau_{\text{wall}} = \frac{8a}{\pi^2} \frac{dp}{dx} \sum_{n=1,3,\dots}^{\infty} (-1)^{\frac{n-1}{2}} \times \left[1 - \frac{\cosh(n\pi z/2a)}{\cosh(n\pi/2)}\right] \frac{(-\sin(n\pi/2))}{n^2}. \quad (20)$$

Figure 4 shows the variation of shear stress along one of the walls of the square duct. It is seen that the maximum shear stress occurs at the center of the wall with only a 1% decrease for 1 mm deviation from the centerline for an 8.5 mm square duct. Compared to the sensing element length of 0.2 mm, we conclude that the spanwise shear stress variation across the sensor is negligible.

3 Experimental set-up

The experiments were carried out in the Interdisciplinary Microsystems Laboratory at the University of Florida. A plane wave tube (PWT) capable of generating purely traveling, acoustic plane waves up to 20 kHz was designed and fabricated. Two series of experiments were performed, one to characterize the response of the PWT, the other to demonstrate the Stokes layer dynamic calibration technique for thermal shear-stress sensors.

Dynamic calibration of the shear-stress sensor first requires a thorough static characterization that includes current-voltage, resistance-temperature and static wall shear stress sensitivity experiments. A detailed description of these experiments and related equipment is given by Cain (1999), Cain et al. (2000), and Sheplak et al. (2002).

3.1 Plane wave tube

A schematic of the acoustic waveguide setup is shown in Fig. 5. The aluminum tube has a length of 1.45 m, a square duct cross-section of 8.5 mm, and a wall thickness of 1.27 cm. Two JBL 2426J-compression drivers

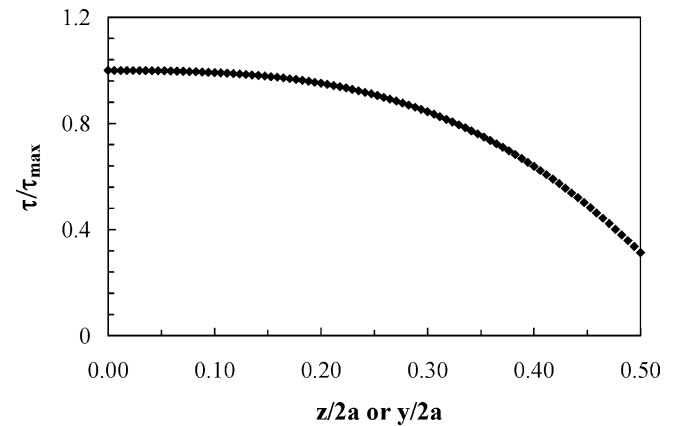


Fig. 4 Mean shear stress variation along a wall of the square duct

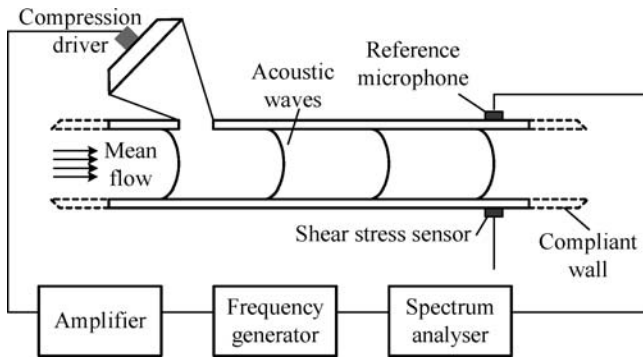


Fig. 5 Schematic of the plane wave tube setup

are attached to the plane wave section via transition ducts with varying inner cross-section. The 1/8" Brüel&Kjær (B&K, Denmark) 4138 microphone and thermal shear-stress sensor are flush mounted on opposite sides of the tube wall at the same axial distance (1.0 m) from the speakers. The B&K 4138 is connected to a B&K 2669 preamplifier and powered by a B&K 2804 power supply. A Stanford Research Systems (Sunnyvale, CA) SR785 spectrum analyzer serves as the signal source and the data collection unit. The speakers are driven by a Techron (USA) 7540 two-channel amplifier. The microphone and the sensor are housed in custom-machined aluminum and Lucite packages, respectively (Chandrasekaran 2000). The Lucite package (Fig. 6) consists of a multi-step circular terrace structure with an O-ring to provide an airtight seal and copper rods to provide front-to-back electrical contacts. The sensor is bonded to the package using fast-cure epoxy within a precision-cut cavity such that flush mounting is achieved. Electrical contact is made between the sensor and copper rods using an ultrasonic ball wire-bonder with 0.025 mm diameter gold wire. When the packaged sensor is mounted in the PWT, the wire bonds are oriented downstream of the active area of the sensor to minimize any disruption to the flow. Both ends of the PWT terminate into compliant tubing to approximate a

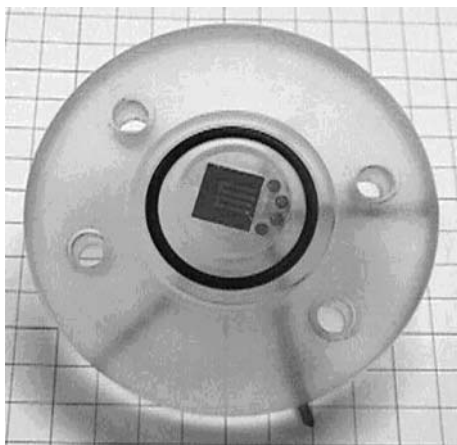


Fig. 6 Shear-stress sensor package

non-reflective acoustic termination (Morse and Ingard 1968). The tubing is a duct with a compliant wall and is intended to dissipate the acoustic energy propagating through it. However, any slight change in acoustic impedance at the interface of the rigid and compliant ducts causes scattering or reflection of the incident acoustic waves (Morse and Ingard 1968). In addition, any change in cross-section of the compliant tubing also modifies the acoustic impedance. The reflected waves propagate in the negative x -direction resulting in a standing wave field in the PWT. If the effect due to the impedance mismatch is strong it could lead to errors in the shear stress measurement, which assumes a purely traveling acoustic wave. However, by measuring the reflection coefficient at the interface of the rigid/compliant wall the assumed form of the pressure perturbation can be modified to include the reflected wave component.

The termination tubing on the inlet (speaker) end of the PWT also serves as the entrance for the mean flow. The flow rate is manually adjusted with a Tescom (USA) 0–103 kPa pressure regulator that is supplied by a compressed air source. The transducers are located at a distance of 120 channel heights from the inlet, ensuring that a fully developed laminar flow is established in the duct (Fox and McDonald 1998). A computational study was conducted using commercial CFD software (FLUENT) to validate this assumption even for the “worst-case scenario” in which large secondary flow disturbances were introduced in the entrance section. The results of the simulations indicate that for a laminar flow the fully developed assumption is valid for sufficiently large distances down the duct, regardless of the inlet condition. While this distance may vary from case to case, for the experiments performed, the sensor was well within a region where the fully developed assumption provided an adequate model for wall shear stress and matched with CFD results to within 0.3%. The termination tubing at the other end of the PWT is open to the atmosphere. Pressure taps located at regular spacing along the length of the test section are used to ascertain the streamwise pressure distribution in the PWT to verify the fully developed incompressible mean flow assumption (Chandrasekaran 2000). The axial pressure-gradient is measured via a 0–124.5 Pa Heise (USA) differential pressure transducer and is used to calculate the mean shear stress induced via Eq. 20. A 30-gauge type K thermocouple is mounted 2.54 cm downstream of the sensor between the top and bottom channel surfaces to measure the fluid temperature. The fluid viscosity and density were then calculated using Sutherland’s formula (White 1991) and the ideal gas law, respectively.

The limiting condition for laminar flow in the PWT was theoretically and experimentally determined. The duct flow is theoretically laminar for $Re < 2300$, corresponding to a wall shear stress of 90 mPa. The transition from laminar to turbulent flow was investigated by monitoring the output voltage of the shear-stress sensor

while increasing the mean flow rate. The sensor voltage began to exhibit significant random fluctuations for mean wall shear stresses > 100 mPa. Once the flow becomes turbulent, Eq. 19 is no longer an accurate representation of the mean velocity profile in the duct.

3.2 Thermal shear-stress sensor

The test device structure consists of a 1500\AA -thick $\times 4\text{ }\mu\text{m}$ -wide $\times 200\text{ }\mu\text{m}$ -long platinum sensing element on top of a 1500\AA -thick silicon-rich silicon nitride membrane. The sensing element is isolated from the bulk silicon substrate via a $200\text{ }\mu\text{m}$ -diameter, $10\text{ }\mu\text{m}$ -deep vacuum cavity (Cain et al. 2000). This structure reduces the sensitivity-limiting thermal conduction into the silicon substrate. The use of a vacuum cavity to reduce substrate conduction effects was first reported by Liu et al. (1994). Each sensor possesses two gold leads at each end of the sensing element to permit 4-point probe characterization exclusive of the effects of the biasing circuitry. The details of the device design, fabrication, and characterization are given by Cain (1999), Cain et al. (2000), and Sheplak et al. (2002). A plan-view scanning electron micrograph (SEM) of the device is shown in Fig. 7, and a cross-sectional schematic is shown in Fig. 8. The sensing element is resistively heated to a temperature greater than the gas temperature defined by the non-dimensional thermal overheat ratio

$$OH = \frac{T_s - T_g}{T_g}, \quad (21)$$

where T_s and T_g are the absolute sensor and gas temperatures, respectively. The convection of heat from the sensor is related to the wall shear stress by the Reynolds analogy (White 1991), and is measured by monitoring changes in the temperature dependent resistance of the sensing element. Constant current sensor excitation and voltage measurements are performed with a Keithley (USA) 2400 source-meter.

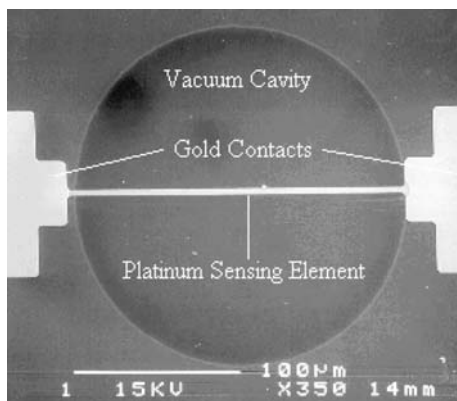


Fig. 7 Plan-view SEM of the active area of the shear-stress sensor

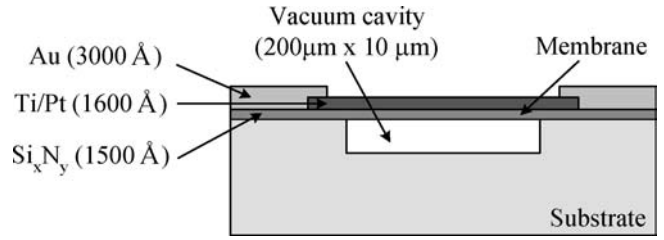


Fig. 8 Cross-sectional schematic of the shear-stress sensor

4 Experimental results

Details of the static calibration of this device are given in Cain (1999) and Sheplak et al. (2002). This section summarizes the results of static and dynamic wall shear stress calibrations of the micromachined thermal shear-stress sensor.

4.1 Static calibration

The non-linear static response of the sensor for varying mean shear stress (10–80 mPa) is shown in Fig. 9. The magnitude of the output response increases with both increasing mean shear stress and overheat ratio. In addition, the degree of non-linearity in the static response is significantly less than that of a hotwire (Comte-Bellot 1976). The local slope of the curve represents the static sensitivity of the device at a particular operating and mean flow condition. As shown in Fig. 10, the static sensitivity increases with increasing overheat ratio, but decreases with increasing mean shear stress. In the following section, results of the dynamic calibration of the thermal shear-stress sensor in a constant current mode of operation are summarized.

4.2 Dynamic calibration

In our experiment, the fluctuating input shear stress is determined from the measured acoustic pressure and

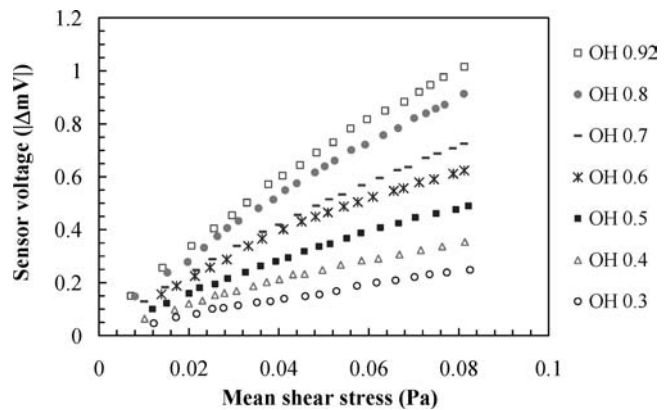


Fig. 9 Static response of the thermal shear-stress sensor for varying overheat ratios

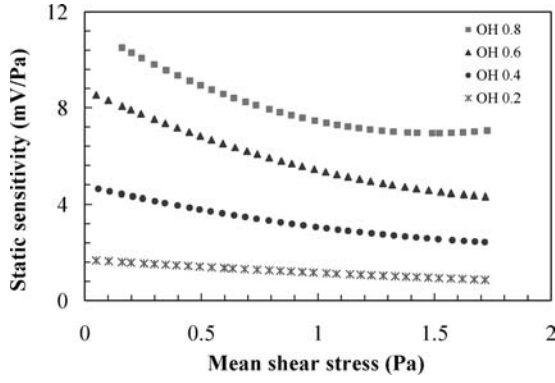


Fig. 10 Static sensitivity of the thermal shear-stress sensor as a function of mean shear stress

frequency as described by Eq. 13. The measured frequency response function is normalized by the static sensitivity, $\partial\bar{V}/\partial\bar{\tau}$ to yield the normalized frequency response function (Sheplak et al. 2001)

$$H(\omega) = \frac{V(\omega)}{\tau(\omega)_{in}} \frac{d\bar{\tau}}{d\bar{V}} \quad (22)$$

Since the magnitude of the shear stress is proportional to the product of the acoustic pressure and the square root of the excitation frequency, a calibration of the compression driver within the PWT was performed. Figure 11 shows a plot of the magnitude of the frequency response of the speaker/PWT system for a constant voltage excitation. To impose a known shear stress on the sensor and avoid acoustic non-linearities, the magnitude of the speaker driving voltage is adjusted to obtain a nearly constant driving pressure perturbation. The oscillations in sound pressure level towards the beginning of the frequency sweep are due to reflections from the ends of the PWT. Although provisions were made to eliminate reflections, the length of compliant tubing (3.5 m) was insufficient, especially at lower frequencies (< 200 Hz).

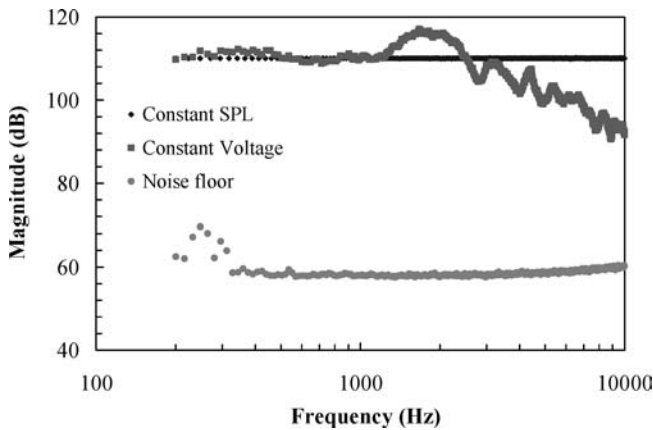


Fig. 11 The response of the compression driver/PWT system to a constant voltage excitation and its correction (measurement noise floor included)

The sensor was dynamically calibrated using a constant amplitude tone (105 dB ref 20 μ Pa), at an overheat ratio of 0.92 and a mean shear stress of 50 mPa. Figure 12 shows the gain factor of the sensor as a function of frequency. The uncompensated sensor displays appreciable sensitivity up to 4 kHz, with the -3 dB point at \sim 600 Hz. Beyond 7 kHz, the response is on the order of the sensor noise floor, which in this case indicates the baseline voltage output of the sensor before the introduction of the acoustic waves. A sound pressure level of 105 dB provides theoretical fluctuating shear stress amplitudes of approximately 2 mPa at 200 Hz to 12 mPa at 7 kHz. For these levels, the local linearization assumption is satisfied (see Fig. 9). To verify the linear relationship between the output voltage fluctuation and the shear stress perturbation, the sensor was excited using acoustic waves of varying amplitude (90–120 dB) at constant frequencies. Figure 13 confirms this linear relationship.

Returning back to Fig. 12, the static and dynamic response should ideally be equal, resulting in a constant gain factor of 0dB. As previously mentioned, the thermal inertia of the shear-stress sensor will cause a roll off in the frequency response function. In Fig. 12, the roll-off in the gain factor appears to be \sim 40 dB/decade, indicative of a highly damped second-order system. Ling and Hubbard (1956) used a 1/2-order system to model the response of a sensor on a semi-infinite medium. The difference in the response of micromachined sensor and the conventional sensor described in Ling and Hubbard (1956) can be explained by the presence of a sealed vacuum cavity. The sealed cavity drastically reduces the unsteady heat conduction into the substrate because the conduction losses are limited to the thin nitride membrane as opposed to the entire substrate.

The phase response of the sensor was also experimentally determined for an overheat ratio of 0.92 and a mean shear stress of 30 mPa and is shown in Fig. 14. The cross-spectrum between the sensor output voltage and the applied acoustic pressure perturbation was

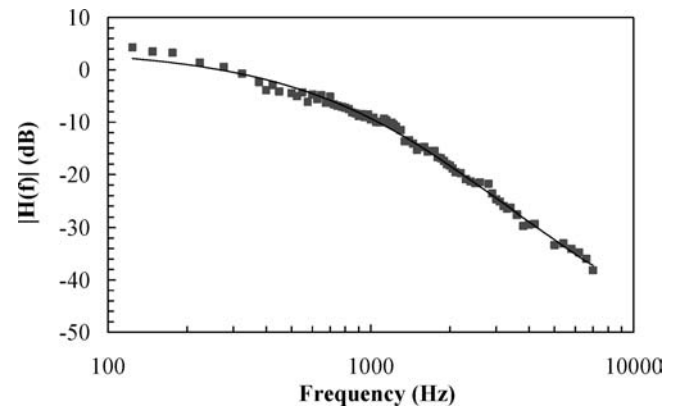


Fig. 12 Gain factor of the sensor frequency response function in response to a 105 dB (ref 20 μ Pa) sine sweep at an overheat ratio of 0.92 and a mean shear stress of 50 mPa

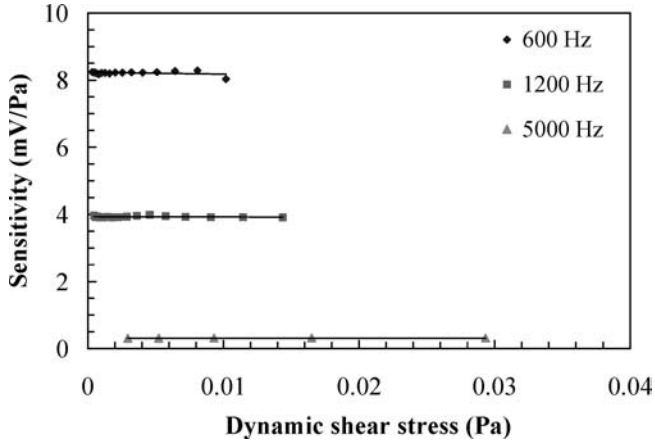


Fig. 13 Linear behavior of the sensor versus oscillating shear stress for a constant overhear ratio of 0.81 and a mean shear stress of 0.03 Pa

taken in order to estimate the phase of the two signals. This follows from the fact that for a linear single-input/single-output system, the frequency response function is (Bendat and Piersol 2000)

$$H(f) = \frac{G_{xy}(f)}{G_{xx}(f)}, \quad (23)$$

where G_{xy} is the cross-spectrum and G_{xx} is the auto-spectrum. Note that the phase of the sensor was not corrected using the theoretical relationship between pressure and shear stress fluctuations. Therefore, at low frequencies, there is a net 45° phase lead as predicted in Eq. 11. The sensor shows no resonant peak and displays a net 180° phase shift, which is characteristic of either a highly damped second-order system or a second-order system with two real poles (i.e., two time constants). The two time constants can be explained as follows. At low frequencies the time response of the sensor will depend on the conduction to the substrate, but at high frequencies the response will only be a function of the heat

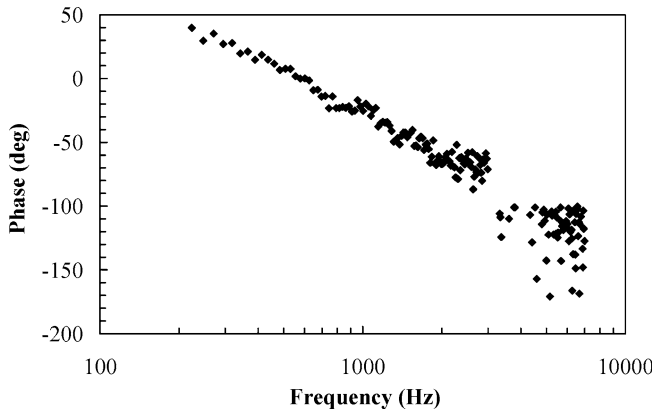


Fig. 14 Phase of the sensor frequency response function in response to a 105 dB (ref 20 μ Pa) sine sweep at an overhear ratio of 0.92 and a mean shear stress of 30 mPa

transfer associated with the film itself (Haritonidis 1989). Measurements obtained beyond 4 kHz display considerable scatter. This is due to the fact that the signal level is near the noise floor of the uncompensated sensor.

5 Conclusions and future work

A method for the direct, in situ, static and dynamic calibration of thermal shear-stress sensors has been described. This technique uses traveling planar acoustic waves superimposed on top of an established laminar mean duct flow to generate a known oscillating shear stress. This technique is novel in that it permits independent variation in the mean and fluctuating shear stresses. The ability to vary these parameters independently is crucial to determine the dynamic response for various mean shear stress levels. The theoretical and practical aspects of this technique were presented as were representative dynamic calibration data for a micromachined thermal shear-stress sensor.

The PWT is capable of generating known sinusoidal shear stress over a frequency range of 2 mPa at 200 Hz to 12 mPa at 7 kHz. The limiting factors in the performance of the PWT include acoustic reflections especially at low-frequencies due to non-ideal termination, giving rise to a small percentage of standing waves and the flow transition to turbulence at low mean shear stress levels (~ 0.08 Pa). The presence of standing waves could, in theory, be accounted for by using the two-microphone method (Jones and Stiede 1997) to decompose the field into incident and reflected waves. In addition, the temperature fluctuation may contribute to the dynamic response of the sensor. Without knowing the dynamic voltage temperature sensitivity of the device, a conservative estimate of the voltage fluctuation due to temperature can be estimated via $V'_T \cong \frac{\partial V}{\partial T} T'$, where

$$V'_T \cong [I_B \bar{R} \alpha] \left[\frac{(\gamma - 1) \bar{T}}{\rho c^2} p' \right]. \quad (24)$$

The first term is the static temperature sensitivity for a fixed bias current I_B , mean sensor resistance \bar{R} at a mean temperature \bar{T} , and α is the thermal coefficient of resistance (Cain et al. 2000; Sheplak et al. 2002). The second term is the isentropic temperature fluctuation associated with an acoustic perturbation, and γ is the ratio of specific heats (Morse and Ingard 1968). As discussed previously, $V'_\tau \cong (d\bar{V}/d\bar{\tau}) \tau'_{\text{wall}}$. For the conditions in Fig. 12, the ratio V'_τ/V'_T varies from 4 at 200 Hz to 25 at 7 kHz. This is a worst-case estimate that will only increase when the thermal boundary layer is accounted for. In any case, a clear understanding of the temperature sensitivity of these devices is required to accurately account for this undesired input.

The work described in this paper is part of an ongoing investigation into the theoretical and experimental aspects of thermal shear-stress sensors. The extension of thermal sensors towards quantitative

turbulence measurements is non-trivial due to the complex conjugated heat-transfer interactions between the sensor and the supporting substrate/membrane. In determining the device sensitivity to shear stress fluctuations, one requires an accurate model of the frequency-dependent conduction term. A model based on one-dimensional heat conduction into a semi-infinite medium is not an accurate representation of this term for the case of a sensor with a sealed vacuum cavity. Clearly, detailed time-resolved flow-field/substrate heat transfer numerical simulations would provide insight into the sensor response to fluctuating shear stress and temperature.

Acknowledgments Financial support for this project was provided by NASA Langley Research Center (Grant#NAG-1-2133) and the Air Force Office of Scientific Research (Contract# F4962-97-1-0507). The thermal shear-stress sensors used to validate the dynamic calibration technique were fabricated in the Microsystems Technology Laboratories (MTL) at the Massachusetts Institute of Technology. We would like to thank Dr. J. Voldman for his help in the sensor fabrication process and TMR Engineering for fabricating the plane wave tube. The last author would like to thank Dr. K. Uno Ingard for his helpful technical discussions.

References

- Bellhouse BJ, Schultz DL (1967) The determination of fluctuating velocity in air with thin film gauges. *J Fluid Mech* 29(2):289–295
- Bellhouse BJ, Schultz DL (1968) The measurement of fluctuating skin friction in air with heated thin-film gauges. *J Fluid Mech* 32(4):675–680
- Bendat JS, Piersol AG (2000) *Random data—analysis and measurement procedures*. Wiley, NY, p 193
- Cain A (1999) Static characterization of a micromachined thermal shear stress sensor. MS Thesis, Department of Electrical and Computer Engineering, University of Florida, Gainesville, FL
- Cain A, Chandrasekaran V, Nishida T, Sheplak M (2000) Development of a wafer-bonded, silicon-nitride membrane thermal shear stress sensor with platinum sensing element. *Technical Digest, Solid-state sensor and actuator workshop*, Hilton Head, SC
- Chandrasekaran V (2000) Dynamic calibration technique for thermal shear stress sensors with variable mean flow. MS Thesis, Mechanical and Aerospace Engineering, University of Florida, Gainesville, FL
- Chew YT, Khoo BC, Lim CP, Teo CJ (1998) Dynamic response of a hot-wire anemometer. Part II: a flush-mounted hot-wire and hot-film probes for wall shear stress measurements. *Meas Sci Technol* 9:764–778
- Comte-Bellot G (1976) Hot-wire anemometry. *Annu Rev Fluid Mech* 8:209–231
- Dowling AP, Williams JEF (1983) *Sound and sources of sound*. Halsted, New York, pp 69–71
- Drake DG (1965) On the flow in a channel due to a periodic pressure gradient. *Quart J Mech Appl Math XVIII(Part I):1–10*
- Fan C, Chao B-T (1965) Unsteady, laminar, incompressible flow through rectangular ducts. *ZAMP* 16:351–360
- Fox RW, McDonald AT (1998) *Introduction to fluid mechanics*, 5th edn. Wiley, New York, p 333
- Freythuth P (1981) Calculation of square wave test for frequency optimized hot-film anemometers. *J Phys E* 14:238–240
- Goldberg HD, Breuer KS, Schmidt MA (1994) A silicon wafer-bonding technology for microfabricated shear-stress sensors with backside contacts. *Technical Digest, Solid-state sensor and actuator workshop*, Hilton Head, SC, pp 111–115
- Haritonidis JH (1989) The measurement of wall shear stress. *Advances in fluid mechanics measurements*. Springer, Berlin, pp 229–261
- Jones MG, Stiede PE (1997) Comparison of methods for determining specific acoustic impedance. *J Acoust Soc Am* 101(5):2694–2704
- Ling SC, Hubbard PG (1956) The hot film anemometer: a new device for fluid mechanics research. *J Aero Sci* 23:890–891
- Liu C, Tai Y, Huang J, Ho C (1994) Surface micromachined thermal shear stress sensor. In: *Proceedings of the ASME symposium on application of microfabrication to fluid mechanics*, Chicago, IL, USA
- Liu C, Huang J-B, Zhu ZA, Jiang F, Tung S, Tai Y-C, Ho C-M (1999) A micromachined flow shear stress sensor based on thermal transfer principles. *J Micro Elec Mech Sys* 8(1):90–99
- Löfdahl L, Gad-el-Hak M (1999) MEMS-based pressure and shear stress sensors for turbulent flows. *Meas Sci Technol* 10:665–686
- Morse PM, Ingard KU (1968) *Theoretical acoustics*. Princeton University Press, Princeton, NJ
- Naughton JW, Sheplak M (2002) Modern developments in shear stress measurement. *Prog Aerospace Sci* 38:515–570
- Ng K-Y (1990) A liquid shear stress sensor using wafer-bonding technology. MS Thesis, Massachusetts Institute of Technology, USA
- O'Brien V (1975) Pulsatile fully developed flow in rectangular channels. *J Franklin Inst* 300(3):225–230
- Oudheusden B, Huijsing J (1988) Integrated flow friction sensor. *Sens Actuat A-Phys* 15:135–144
- Padmanabhan A, Goldberg HD, Schmidt MA, Breuer KS (1996) A wafer-bonded floating-element shear stress microsensor with optical position sensing by photodiodes. *J Micro Elec Mech Syst* 5(4):307–315
- Padmanabhan A, Sheplak M, Breuer KS, Schmidt MA (1997) Micromachined sensors for static and dynamic shear stress measurements in aerodynamic flows. *Technical Digest, Transducers 1997*, Chicago, IL, USA, pp 137–140
- Pan T, Hyman D, Mehregany M, Reshotko E, Garverick S (1999) Microfabricated shear stress sensors, part 1: design and fabrication. *AIAA J* 37(1):66–72
- Panton RL (1996) *Incompressible flow*, 2nd edn. Wiley, NY, pp 267–270
- Perry AE, Smits AJ, Chong MS (1979) The effects of certain low frequency phenomena on the calibration of hot wires. *J Fluid Mech* 90:415–431
- Schmidt MA, Howe RT, Senturia SD, Haritonidis JH (1988) Design and calibration of a microfabricated floating-element shear-stress sensor. *IEEE T Electron Dev* 35:750–757
- Sheplak M, Padmanabhan A, Schmidt MA, Breuer KS (2001) Dynamic calibration of a shear stress sensor using stokes layer excitation. *AIAA J* 39(5):819–823
- Sheplak M, Chandrasekaran V, Cain A, Nishida T, Cattafesta L (2002) Characterization of a micromachined thermal shear stress sensor. *AIAA J* 40(6):1099–1104
- Tennekes H, Lumley JL (1972) *A first course in turbulence*. MIT Press, Cambridge, MA
- White FM (1991) *Viscous fluid flow*, 2nd edn. McGraw-Hill, NY